IOP Conf. Series: Materials Science and Engineering **891** (2020) 012014 doi:10.1088/1757-899X/891/1/012014

The microanalysis of iron and sulphur oxidation states in silicate glass - Understanding the effects of beam damage

E C Hughes[1,2], B Buse[1], S L Kearns[1], R A Brooker[1], D Di Genova[3], G Kilgour[4], H M Mader[1] and J D Blundy[1]

[1] University of Bristol, School of Earth Sciences, Wills Memorial Building, Queens Road, Bristol, BS8 1RJ, Great Britain
[2] California Institute of Technology, Division of Geological and Planetary Sciences, 1200 E. California Blvd., 91125 Pasadena, CA, U.S.A.
[3] Technische Universität Clausthal, Institut für Nichtmetallische Werkstoffe, Zehntnerstrasse 2a, 38678 Clausthal-Zellerfeld, Germany
[4] GNS Science, Wairakei Research Centre, 114 Karetoto Road, RD4, 3384 Taupo, New Zealand

E-mail: ehughes@caltech.edu

Abstract. Quantifying the oxidation state of multivalent elements in silicate melts (e.g., Fe^{2+} versus Fe^{3+} or S^{2-} versus S^{6+}) is fundamental for constraining oxygen fugacity. Oxygen fugacity is a key thermodynamic parameter in understanding melt chemical history from the Earth's mantle through the crust to the surface. To make these measurements, analyses are typically performed on small (<100 µm diameter) regions of quenched volcanic melt (now silicate glass) forming the matrix between crystals or as trapped inclusions. Such small volumes require microanalysis, with multiple techniques often applied to the same area of glass to extract the full range of information that will shed light on volcanic and magmatic processes. This can be problematic as silicate glasses are often unstable under the electron and photon beams used for this range of analyses. It is therefore important to understand any compositional and structural changes induced within the silicate glass during analysis, not only to ensure accurate measurements (and interpretations), but also that subsequent analyses are not compromised. Here, we review techniques commonly used for measuring the Fe and S oxidation state in silicate glass and explain how silicate glass of different compositions responds to electron and photon beam irradiation.

1. Introduction

Magmas are a complex and evolving mix of bubbles, crystals, and melt, where the abundance and composition of these phases changes significantly during ascent. Such changes have implications for how the magma flows and hence eruption style, which has the potential for developing methods to predict eruption style from volcano monitoring data. This requires quantifying the parameters that affect the chemical and physical properties of the magma. Natural silicate melts cover a wide range of compositions, containing ~45 - 75 wt% SiO_2 and varying amounts of TiO_2, Al_2O_3, Fe_2O_3, FeO, CaO, MgO, MnO, Na_2O, K_2O, and P_2O_5 (Fig. 1a). In addition, silicate melts may contain volatiles such as H_2O, CO_2, S, and halogens (e.g., Cl, F, Br, etc.). To cover the range of compositional effects, two

extreme endmembers are considered (Fig. 1a): one is basaltic, which is low-silica (~50 wt% SiO_2), Fe-rich (~8 wt% Fe), and alkali-poor (<5 wt% Na_2O+K_2O); whilst the other is rhyolitic, which is high-silica (~70 wt% SiO_2), Fe-poor (~2 wt% Fe, except pantellerite which contains ~6 wt% Fe), and alkali-rich (~8 wt% Na_2O+K_2O).

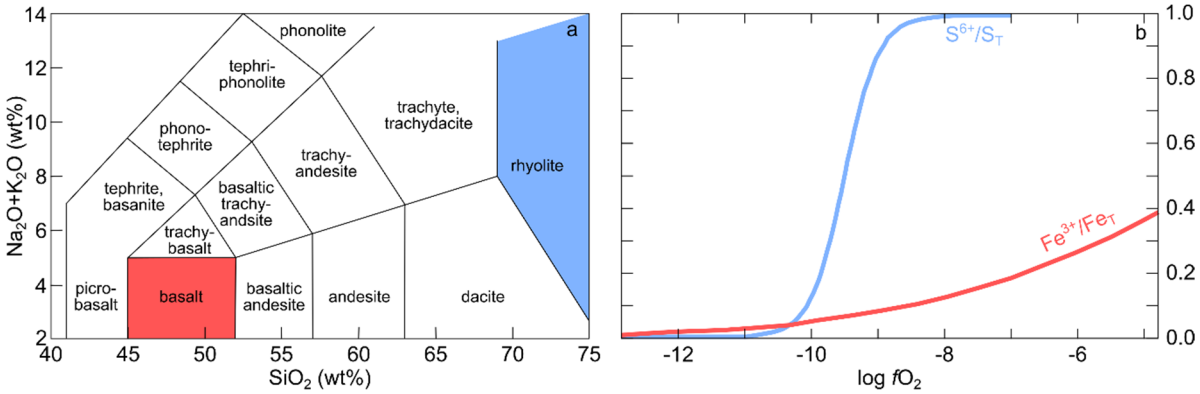

Figure 1. a) Na_2O+K_2O against SiO_2 labelled by composition, where basalt (red) and rhyolite (blue) are shaded. b) Typical effects of oxygen fugacity (fO_2) on melt Fe (Fe^{3+}/Fe_T) [1] and S (S^{6+}/S_T) [2] oxidation state.

Oxygen fugacity (fO_2) is equivalent to the activity of oxygen in a system. It is a key thermodynamic parameter that controls the oxidation state of multivalent elements within the magma (mainly Fe and S, but also Mn, Cr, V, Ce, and Eu; [1, 3, 4]). Figure 1b illustrates how fO_2 typically controls the valency of Fe (Fe^{2+} and Fe^{3+}) and S (S^{2-} and S^{6+}), which can have a major effect on the physical and chemical properties of the magma. The fO_2 affects volatile solubility, mineral-melt equilibria (e.g., phase assemblage), and magma viscosity, as well as controlling the composition of exsolved vapour and even the formation of economic ore bodies (e.g., [5-11]). The fO_2 varies between different magmatic systems, often related to tectonic setting, but can also be perturbed by processes such as fractionation and degassing (e.g., [12, 13]). For these reasons fO_2 is an important parameter to constrain when investigating the evolution of magmatic systems; it can be inferred by measuring the melt Fe or S oxidation state, i.e., the ratio of the reduced to oxidised species (Fig. 1b). Melt inclusions (tiny pockets of glass 1 - 500 µm in diameter in crystals) or matrix glass (final melt composition) are commonly analysed for this purpose (Fig. 2). Melt inclusions form when melt is trapped during crystal growth, providing a unique sample of the melt, which quenches to a glass upon eruption [14].

Multiple microanalytical techniques are often used to analyse melt inclusions and matrix glass due to the wide variety of elements present (at variable concentrations) and range of information required (including concentration, oxidation state, and isotope ratio, e.g., [15]). By necessity, this means that the same area of glass may be analysed multiple times. Interaction of the beam (i.e., electron or photon) with the glass during analysis can cause changes to the composition and structure of the glass, which is broadly referred to as 'beam damage'. As a result, it is important to understand if, and to what extent, these measurements affect the glass and whether subsequent analyses are compromised. The cause of beam damage and the subsequent effects depend on the type and conditions of analysis, as well as the sample (e.g., composition and thickness). Hence, each section covers a separate technique commonly used to analyse Fe and S oxidation state in silicate glass (Fig. 3; Sections 2-6). Sections begin with a brief description of how the technique is used to quantify the Fe (and S if applicable) oxidation state, followed by the observations and possible mechanisms of beam damage. Mitigation strategies and recommendations for multi-technique analytical protocols are suggested in Section 7.

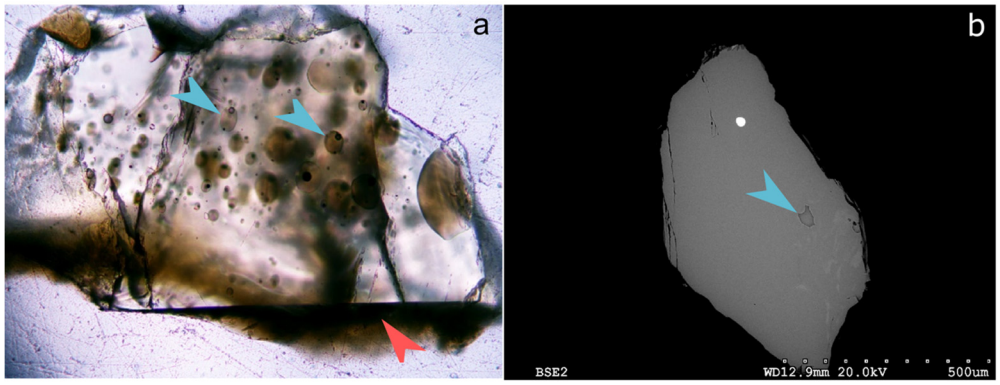

Figure 2. a) Photomicroscope (transmitted light) image of an olivine crystal containing melt inclusions (blue, bottom-right arrows – not all melt inclusions are indicated for clarity) and matrix glass (red, top-left arrow), both of which are brown. b) Backscattered electron image of a pyroxene crystal containing a melt inclusion (blue, bottom-right arrow), which is dark grey.

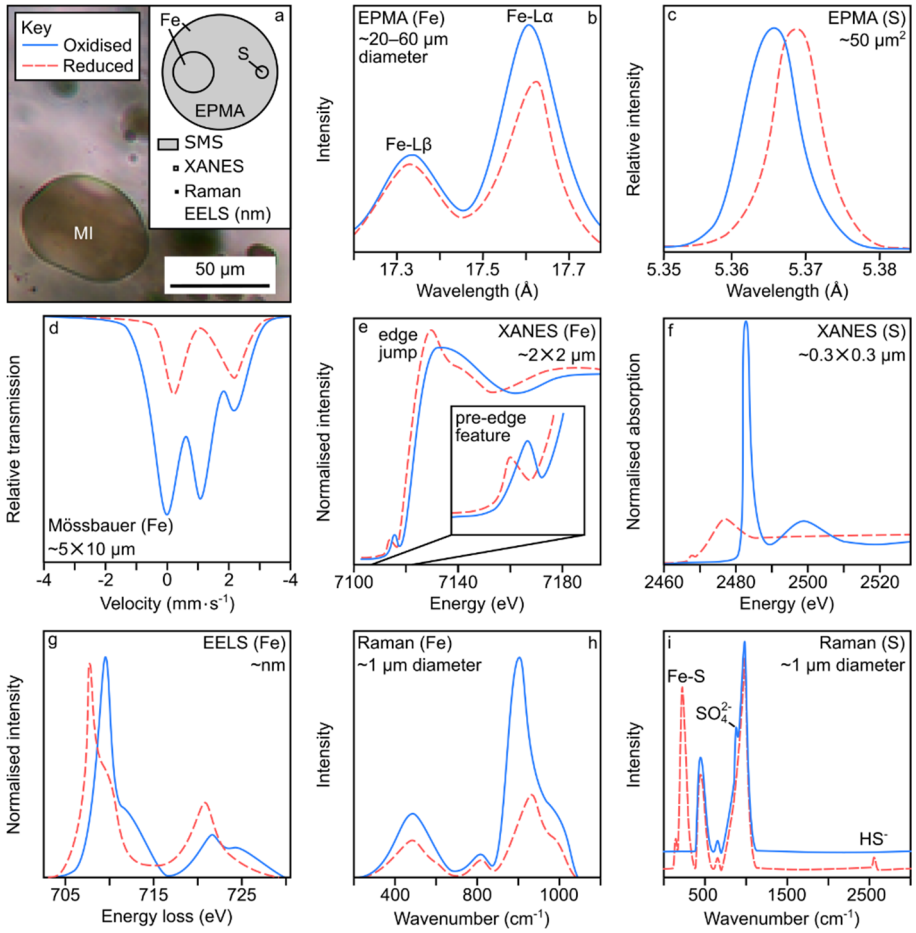

Figure 3. a) Olivine-hosted melt inclusion (MI) with the spatial resolution of the different techniques shown for comparison (spatial resolutions are also quoted on each panel). Schematic spectra for oxidised (solid, blue line) and reduced (dashed, red line) samples for b) Fe-L using EPMA [16], c) S-Kα using EPMA [17], d) Fe using Mössbauer [18], e) Fe K-edge using XANES [18], f) S K-edge using XANES [2], g) Fe L-edge using EELS [19], h) Fe using Raman [20], and i) S using Raman [21].

2. Electron probe microanalysis (EPMA)

2.1. Technique

Measuring Fe oxidation state with EPMA uses the Fe-L X-ray lines, which are produced by the 3d → 2p electron transition (Fig. 3b). The change in position and intensity of the Fe-Lα (~17.6 Å) and Fe-Lβ (~17.3 Å) peaks are a function of Fe oxidation state, as well as the concentration of Fe and its coordination [22, 23]. This is caused by changes in the energy of the 3d electron shell due to bonding, as well as changes in self-absorption of the emitted X-rays [24, 25]. For instance, the intensities of the Fe-L peaks are higher if the glass contains more Fe or if the Fe is more oxidised (i.e., Fe^{2+}/Fe_T decreases) [16]. Additionally, the Fe-L peak positions occur at higher wavelengths for higher Fe concentrations or if the Fe is more reduced (i.e., Fe^{2+}/Fe_T increases) [16]. Nonetheless, careful calibration of these effects can enable the quantification of Fe^{2+}/Fe_T, with an error of ± 0.1 absolute on Fe^{2+}/Fe_T [16, 25, 26].

There are two methods to exploit these changes: the 'peak shift' and 'flank' methods [27]. The peak shift method correlates the Fe-Lα peak position (measured by scanning the spectrometer over the X-ray peak of interest, commonly referred to as a 'wavescan') at a given Fe concentration with Fe^{2+}/Fe_T [28]. The flank method correlates the change in the intensity ratio of positions on the low wavelength flank of Fe-Lα (Fe-$L\alpha_f$) and the high wavelength flank of Fe-Lβ (Fe-$L\beta_f$) (Fe-$L\beta_f$/Fe-$L\alpha_f$) with the Fe^{2+} content of the glass (which is converted to Fe^{2+}/Fe_T using known Fe_T) [23, 27, 29]. The flank method has greater sensitivity than the peak shift method because it utilises both changes in peak position and intensity [27]. Silicate glass standards of similar composition (e.g., basalt or pantellerite) or garnets (andradite and almandine) can be used for calibration [16, 26]. The presence of Fe-bearing nanosized crystals (i.e., nanolites) in the glass prevents quantification of Fe oxidation state using EPMA, likely because the signal is a mix of the Fe in the glass and the nanolites (Fig. 4).

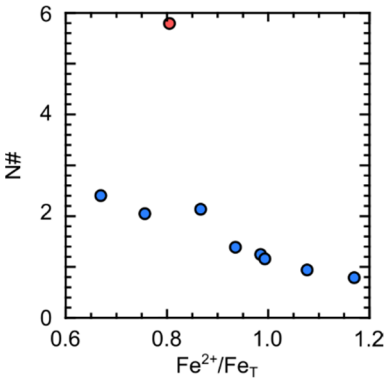

Figure 4. Quantity of nanolites measured by Raman (degree of nanolitisation, N#, defined by [30]) against Fe^{2+}/Fe_T measured using EPMA on natural melt inclusions. The negative correlation between N# and Fe^{2+}/Fe_T (excluding one outlier in red) implies the presence of nanolites changes the intensity and/or peak positions of the Fe-L lines compared to silicate glass. This prevents quantification of the Fe oxidation state using EPMA and can lead to spurious values (i.e., $Fe^{2+}/Fe_T > 1$).

The S-Kα peak (2p → 1s) shifts to higher wavelengths with increased proportion of reduced sulphur due to the lower bond energies of reduced sulphur (Fig. 3c) [31]. The peak shift method is used to quantify S oxidation state (S^{6+}/S_T), although it cannot distinguish S^{4+} from a combination of S^{2-} and S^{6+} [32-35]. Mineral end-members (e.g., barite and troilite) are used to define the peak positions of S^{2-} and S^{6+} and a linear variation in S^{6+}/S_T is assumed between these two positions. An error of ±3.5 % on sulphate can be achieved using this technique [34].

2.2. Beam damage

Electron probe beam damage has been well documented in a variety of studies, as summarised below (beam conditions of 15 - 30 kV accelerating voltage, 4 - 30 μm beam diameter, 2 - 500 nA beam current). Silicate glass is an insulator, hence during EPMA incident electrons are trapped in the band gap within

the sample [36]. This generates a region of negative charge below the interaction volume, which produces an electric field within the glass [37]. This electric field causes a variety of changes to the glass, such as cation migration and oxidation/reduction of Fe and S (Fig. 5). In all cases, increasing the electron beam density (i.e., decreased beam diameter, increased beam current, or decreased accelerating voltage) increases the rate or severity of the beam damage as this increases the magnitude of the electric field produced [16, 38-40].

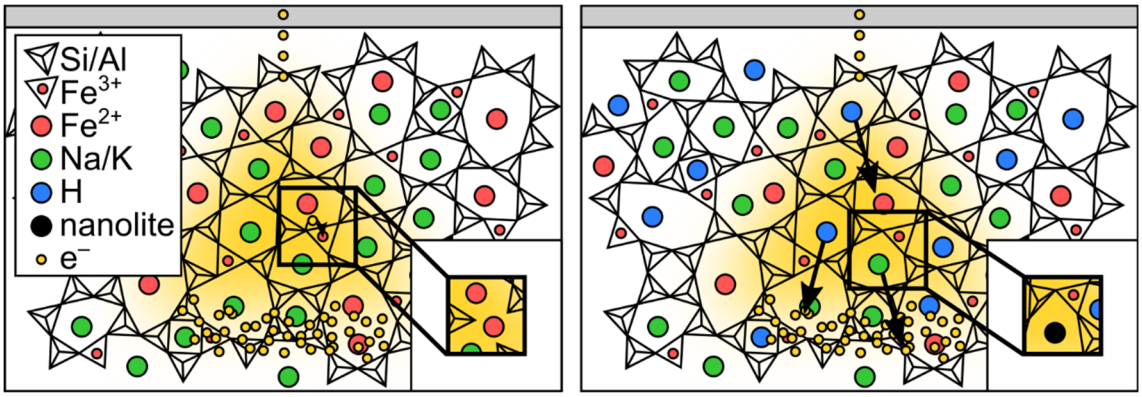

Figure 5. Schematic diagram of the processes occurring during electron beam irradiation in an electron probe. The silicate glass is carbon-coated (shaded grey) in a vacuum and contains mobile elements (e.g., H – blue circle, Na and K – green circles), variably oxidised Fe (Fe^{3+} – red circle in triangle, Fe^{2+} – red circle), and other glass components (Si and Al – triangles) (glass structure based on [41]). During electron beam irradiation, electrons (small yellow circle) are trapped building up a region of negative charge above which an electric field (yellow region) is present. a) In anhydrous silicate glass, electrons are transferred from O to Fe^{3+} causing reduction if there is sufficient Fe. b) In hydrous silicate glass, positively charged mobile ions migrate towards the negative charge at depth, which can oxidise Fe and precipitate Fe-bearing nanolites (black circle).

The electric field results in the migration of mobile cations (e.g., Na^+, H^+, K^+) towards the region of negative charge (Fig. 5b). This causes the concentration of mobile cations (e.g., H, Na, and K) to decrease with time, which can be observed using time-dependent intensity (TDI) measurements of X-rays using EPMA (e.g., decreasing K-Kα intensity; Fig. 6a) and Raman maps of the analysed area (decrease in height of H_2O peak at ~3,500 cm^{-1}, Fig. 6d) [39, 42]. These ions are known to migrate into the sample as subsequent secondary ion mass spectrometry (SIMS) depth profiles show a decrease in the concentration of mobile elements (e.g., H^+, Li^+, Na^+, and K^+) towards the surface (Fig. 6e) [38]. The exception to this is H in rhyolite, which increases in concentration towards the surface, implying OH^- (which is negative and hence would migrate away from the region of negative charge) rather than H^+ migration [38]. Immobile ions remain static and therefore their concentration increases, as observed using EPMA TDI measurements (e.g., Si, Al, Fig. 6b) [39, 42]. At cryogenic temperatures (-190 °C) the mobile cations are unable to migrate in response to the electrostatic field [40]. The rate or severity of migration increases with decreasing atomic radius of the mobile element (i.e., H > Li > Na > K), because smaller ions migrate faster, and increasing SiO_2 content of the glass (rhyolite > dacite > andesite) due to increasing polymerisation [38-40].

The migration of mobile cations leaves behind O which can oxidise Fe, hence hydrous basalts and alkali-rich glasses are able to oxidise (Fig. 6c) [16, 43]. With continued oxidation, nanolites of magnetite and even haematite can precipitate, as observed using Raman spectroscopy (increase in height of magnetite peak at ~670 cm^{-1}, Fig. 6d) [16]. Additionally, secondary electron scanning electron

microscopy imaging has shown changes in the surface morphology of irradiated glass, which is interpreted to result from oxygen bubbles outgassing from the sample [43]. The rate of oxidation increases with increasing H_2O concentration because the rate of diffusion of mobile cations is faster at higher H_2O concentrations [16, 38].

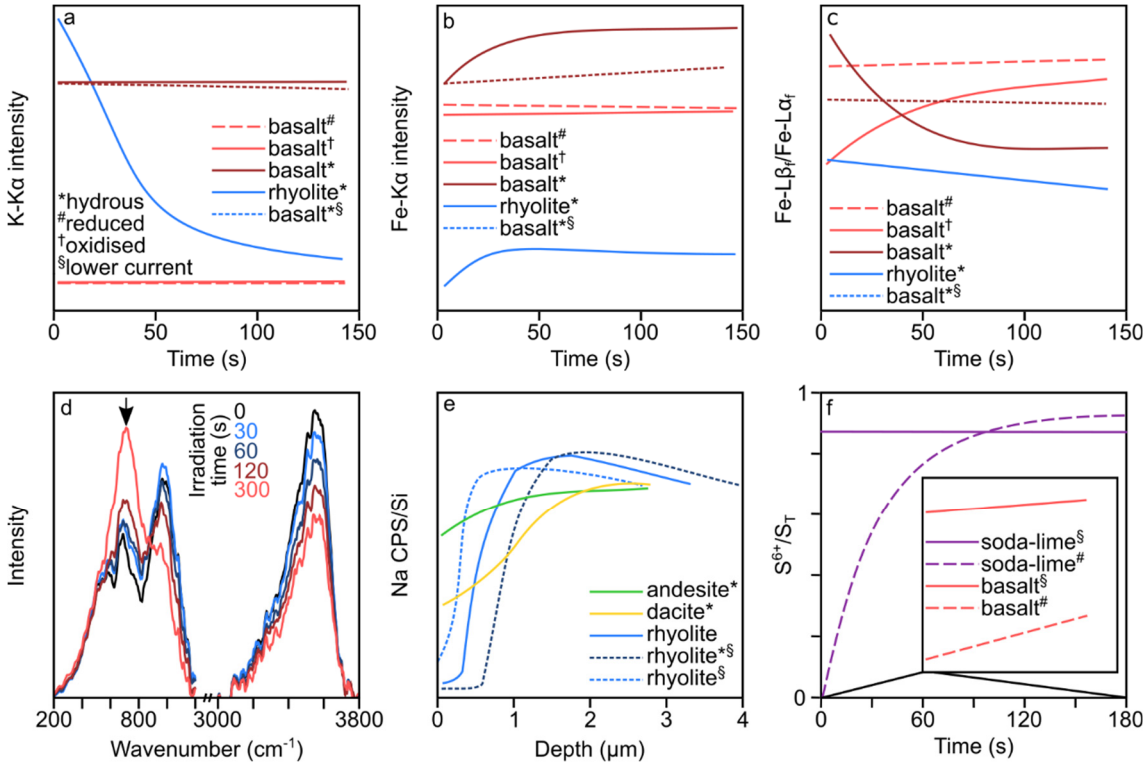

Figure 6. Changes in glass composition and structure during electron beam irradiation in an electron probe. EPMA TDI data from [16] for a) migration of a mobile element (K), b) grow-in of an immobile element (Fe), and c) changes in Fe oxidation state. d) Raman data over time for a nanolite-bearing hydrous basalt showing the silicate peak region (200 - 1,400 cm^{-1}, magnetite is the peak at ~670 cm^{-1} shown by the arrow) and H_2O peak (3,000 - 3,800 cm^{-1}). e) SIMS data from [38] for Na. f) EPMA TDI data from [21, 34] for oxidation of S. Line colour indicates glass composition (basalt = red, andesite = green, dacite = yellow, rhyolite = blue, and Fe-free soda-lime = purple), where darker hues indicate the glass is hydrous*; dashed line indicates reduced# glass, solid line indicates oxidised† glass, and dotted line indicates lower beam current§ used for analysis.

Fe reduction likely occurs in the glass via electron transfer from O to Fe^{3+} but is only observed when the rate of oxidation is slow (Fig. 5a) [16, 44]. Anhydrous basalts can reduce because there are insufficient mobile cations (e.g., H^+) to migrate and leave behind oxygen [16]. The rate of reduction is controlled by the concentration of Fe^{3+} remaining, resulting in an exponential trend in oxidation state with time, and increases with lower initial Fe^{2+}/Fe_T (Fig. 6c) [16].

Anhydrous and hydrous rhyolites (with low and high Fe), and hydrous basalts containing nanolites, do not appear to change oxidation state using TDI EPMA under beam densities that cause damage in hydrous basaltic glass [16]. On the other hand, there was an increase in the quantity of magnetite and haematite nanolites observed using Raman after EPMA for pantelleritic and nanolite-bearing hydrous basaltic glass, which implies oxidation did occur but was too fast to be observed using EPMA [16].

No nanolites were observed for hydrous rhyolitic glass with low Fe, hence these did not oxidise [16]. Therefore, either OH^- rather H^+ migration occurred (as suggested by SIMS), which would not leave oxgyen behind for oxidation, or their Fe contents are too low for oxidation to proceed [16, 38].

The mechanism for changes in S oxidation state is probably similar to Fe, although oxidation and reduction proceed via the formation of S^{4+} as observed using XANES analysis of the S K-edge (Fig. 6f) [33]. Less data are available on the compositional controls on the rate and direction of redox change. TDI measurements of S oxidation state using EPMA show that the rate of oxidation appears to increase with decreasing Fe concentration, increasing S concentration, and decreasing initial S^{6+}/S_T [17, 21, 34, 35]. Extremely rapid oxidation has been observed for very S-rich but Fe-free glass, which implies these redox changes are coupled and that Fe more readily changes redox state than S [17, 21]. Conversely, reduction occurs for initially oxidised glasses [45].

3. X-ray absorption near-edge structure (XANES) spectroscopy

3.1. Technique

XANES is an X-ray absorption spectroscopy technique that uses changes in the pre-edge structure of the Fe K-edge (1s → 3d) that are caused by changes in the Fe concentration, coordination, and oxidation state (Fig. 3e). Broadly, with decreasing Fe^{2+}/Fe_T, the edge jump (~7,120 eV) and crest move to higher energies and the higher energy pre-edge feature increases (and the lower energy pre-edge feature decreases) in intensity [18]. There are a variety of ways of quantifying the Fe oxidation state from XANES spectra, such as the centroid position or height ratio of the pre-edge features (after fitting the spectra with a linear function and damped harmonic oscillator) and principal component analysis [18, 46, 47]. Very high precision on Fe^{2+}/Fe_T measurements (± 0.0045 - 0.013 absolute [18, 47]) can be obtained using well-characterised standards, but data processing must be consistent between different datasets for robust comparison. Additional complexity, such as contamination from the host-mineral, crystallinity within the glass, or differences in the matrix glass composition, can severely compromise oxidation state quantification.

Similarly, the S oxidation state can be quantified using the S K-edge. In addition to S^{2-} and S^{6+}, S^{4+} that is produced by beam damage can also be detected (Fig. 3f) [2, 17]. The proportion of each species can be quantified by comparing to reference spectra, resulting in ± 5 % total error on S^{6+}/S_T [21].

3.2. Beam damage

Fewer studies have investigated beam damage during XANES compared to EPMA, and hence less is known about the compositional controls. Data described below are for typical beam conditions, which vary depending on the synchrotron used for data collection (10^3 - 10^{11} photons·s^{-1}·μm^{-2} flux). Time-dependent measurements at a single energy (e.g., the second pre-edge multiplet) or repeated measurements on the same spot during XANES can be used to monitor changes in Fe or S oxidation state. The mechanisms for beam damage during XANES are different to EPMA, resulting from the energy transferred from the photon beam to the glass rather than in response to an electric field (Fig. 7).

Reduction of Fe is thought to occur by charge transfer from localised defects in the glass to neighbouring Fe^{3+}, causing reduction to Fe^{2+} (Fig. 7a) [48]. The region of localised defects created by the high energy photon beam causes cation displacement [48]. The resulting anionic vacancies produce visible grey marks in the glass after irradiation [48]. This was inferred by Gonçalves Ferreira *et al.* [48] as silica-rich (soda-lime) glass with low Fe concentrations (< 5,000 ppm Fe) reduced over time with no change in Fe coordination (Fig. 8a). The rate of reduction increases with decreasing Fe concentration, but the absolute amount of Fe reduced is the same regardless of the total Fe content (Fig. 8a). At elevated temperatures these defects relax, therefore the reduction of Fe can be reversed by heating the sample and no Fe reduction occurs when the measurements were made at higher temperatures (~500 °C) [48].

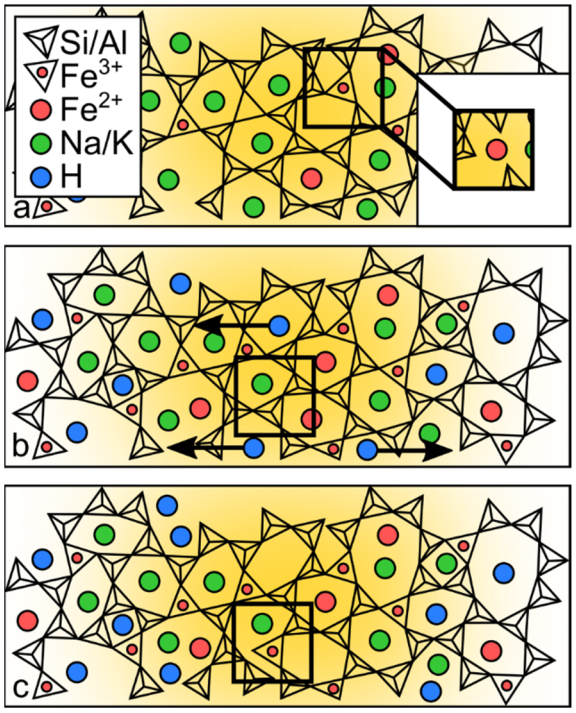

Figure 7. Schematic diagram of the processes occurring during photon beam irradiation in a synchrotron. The silicate glass sample contains H (blue circle), variably oxidised Fe (Fe^{3+} – red circle in triangle, Fe^{2+} – red circle), and other glass components (Si and Al – triangle, Na and K – green circle) (glass structure based on [41]). a) The photon beam creates defects in the glass, which provides the charges to reduce Fe^{3+} to Fe^{2+}. b) The photon beam irradiation breaks O–H bonds and H migrates faster out of the analysis area than O, and c) this O oxidises Fe^{2+} to Fe^{3+}.

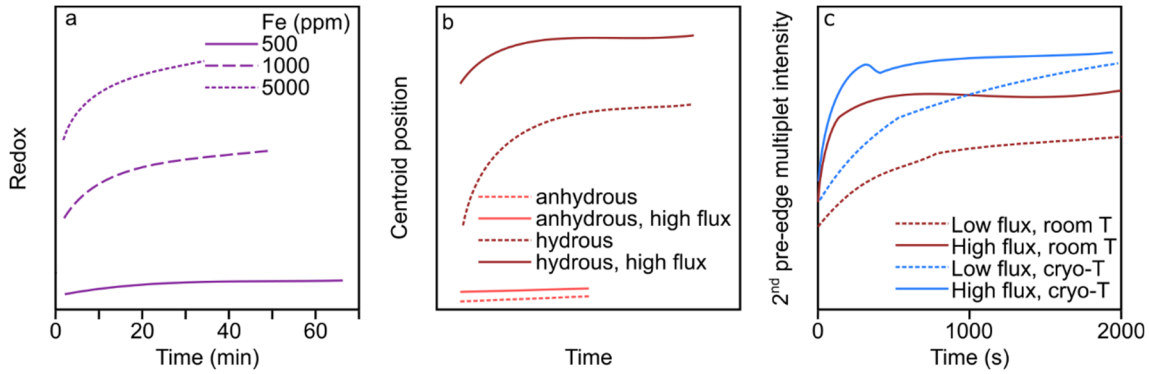

Figure 8. Changes in glass composition during photon beam irradiation in a synchrotron during XANES spectroscopy: a) Fe reduction with time from [48] for Fe-poor, soda-lime glass, b) Fe oxidation with time from [49] for anhydrous and hydrous basaltic glass at low and high photon fluxes, and c) Fe oxidation with time from [49] for hydrous basaltic glass for low and high photon fluxes at room and cryogenic temperatures.

On the other hand, anhydrous basaltic glass (i.e., high Fe concentration) shows no change in Fe oxidation state with time (Fig. 8b) [18, 46, 50]. Anhydrous and hydrous dacitic to rhyolitic glass also show no change in Fe oxidation state with time [51]. The latter was deduced from the lack of change between repeated analyses, rather than time-dependent measurements, and therefore the change may already have occurred within the first analysis [49, 51].

Cottrell *et al.* [49] investigated beam damage to hydrous basaltic glass (Fig. 8b). They observed that during analysis the Fe^{3+} multiplet increases in intensity, the Fe^{2+} multiplet decreases, and the white line shifts to higher energy, which implies oxidation of Fe^{2+} to Fe^{3+} rather than increased 3d-4p hybridisation. The mechanism proposed for Fe oxidation involves H_2O ($2FeO_{(glass)} + H_2O_{(glass)} \rightarrow Fe_2O_{3(glass)} + H_{2(gas)}$)

[21, 49]. Photon radiation breaks the O–H bonds (Fig. 7b), H then outgases from the sample leaving behind O to oxidise Fe (Fig. 7c). Oxidation was faster at higher photon fluxes, lower temperatures (cryogenic, -190 °C), higher H_2O concentrations or more reduced samples, and was permanent (Fig. 8c). Fourier transform infra-red (FTIR) spectra of the analysed area showed a reduction in H_2O concentration [49]. The increased rate of oxidation observed at cryogenic temperatures for Fe suggests that O cannot diffuse at such low temperatures and hence the oxidation rate is increased [49].

The data for S are more complicated, as different beamlines appear to produce different results, likely due to their different beam intensities [17]. Initially oxidised glass reduces over time and S^{4-} is observed, where the rate is controlled by the beam conditions and also increases with H_2O present, whereas partially or completely reduced samples do not change oxidation state [17, 33]. On the other hand, S oxidation is seen at higher intensity beamlines, especially when H_2O is present in the glass, and a similar reaction to Fe oxidation is proposed ($S^{2-}_{(glass)} + 4H_2O_{(glass)} \rightarrow SO_4^{2-}_{(glass)} + 4H_{2(gas)}$) [33]. The oxidation state of S becomes more stable with decreasing S/Fe ratio of the glass, again suggesting coupled redox changes as for EPMA [21].

4. Electron energy loss spectroscopy (EELS)

4.1. Technique

EELS in a transmission electron microscope (TEM) affords the opportunity to measure Fe oxidation state at sub-nanometre scale. The Fe L-edge (2p → 3d) has two distinct sub-edges, whose shape and position are dependent on Fe oxidation state, symmetry, and coordination state (Fig. 3g) [19]. Gaussian fits to the spectra could provide a way to quantify the Fe oxidation state, but it can prove difficult to find standards that are homogeneous at the analysis scale, which currently precludes quantification [19].

4.2. Beam damage

Burgess *et al.* [19] studied beam damage of silicate glass during EELS (beam conditions of 60 - 100 kV accelerating voltage and 0 - 7 × 10^6 $e \cdot nm^{-2} \cdot s^{-1}$ dose). They observed glass density changes and the concentration of most elements decreases in the analysed region, except for Si which is conserved and therefore increases in its relative proportion. Fe oxidation and reduction were observed, but there is no clear relationship between rate of redox change and sample thickness, electron dose rate, or total dose. Generally, reduced samples become more oxidised with increasing dose, whilst at the highest doses reduction occurs. Magnetite nanolites were observed in the glass, but it is not certain whether these were present before analysis. Additionally, during sample preparation and loading into the TEM, surface oxidation occurred.

These observations illustrate that the damage is caused by an electric field in the glass, but via a different mechanism than during EPMA. For EELS, as the sample is very thin, the emission of secondary and auger electrons generates a region of positive charge in the analysis area, generating an electric field (Fig. 9a) [19, 37]. Electrons can hop between Fe^{2+} and Fe^{3+}, which may cause both reduction and oxidation (Fig. 9b) [19]. The region of positive charge causes the cations to migrate out of the analysis area, reducing their concentration (Fig. 9c) [19]. Fe^{2+} can migrate faster than Fe^{3+}, hence this causes oxidation (Fig. 9d) [19]. During sample preparation, initially oxidised samples have a thinner oxidised layer as there is less driving force for oxidation [19].

5. Raman spectroscopy

5.1. Technique

Raman spectroscopy measures the shift in wavelength of monochromatic light due to inelastic scattering of the incident photons when they interact with molecular vibrations, where the electron cloud is deformable. Uniquely, Raman (in confocal mode) can focus the beam at depth on unexposed areas of glass, which means melt inclusions do not have to be exposed at the surface for analysis [52].

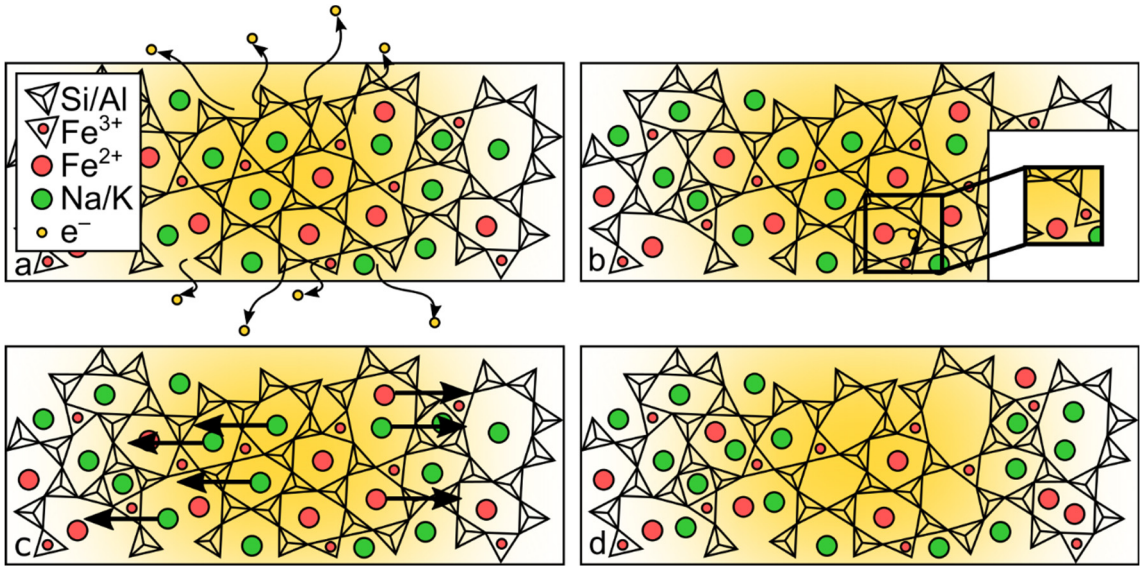

Figure 9. Schematic diagram of the processes occurring during electron beam irradiation in a TEM. The silicate glass sample is sufficiently thin to be transparent to electrons and contains variably oxidised Fe (Fe^{3+} – red circle in triangle, Fe^{2+} – red circle) and other glass components (Si and Al – triangles, Na and K – green circle) (glass structure based on [41]). a) Electron beam irradiation creates secondary electrons (small, yellow circle), which generates a region of positive charge (yellow region). b) Electrons hop between Fe^{2+} and Fe^{3+} causing changes in oxidation state. c) Most cations migrate away from the positive charge, and (d) as Fe^{2+} migrates faster than Fe^{3+} oxidation occurs.

Unfortunately, fluorescence can cause difficulties in processing spectra [21]. There are various bands sensitive to the Fe oxidation state of silicate glass, which increase in intensity with increasing Fe^{3+} content at constant Fe concentration [20, 53] (Fig. 3h). Both spectral deconvolution [53] and empirical calibrations based on ideal mixing equations [20] have been used to quantify Fe^{2+}/Fe_T. The sensitivity of the technique and calibration are composition dependent, with pantellerite being more sensitive than basalt, and the H_2O content also being important.

For sulphur, specific peaks in the glass spectra are produced due to different bonding environments associated with S such as Fe-S (372 cm^{-1}), SO_4^{2-} (990 cm^{-1}), and SH^- (2,574 cm^{-1}) (Fig. 3i) [21]. This provides greater information about the speciation of S than EPMA or XANES as information on the cation the sulphur is bonding to is also given. Unfortunately, Raman is relatively insensitive to sulphur, therefore, significant quantities of S may be required to see these peaks above the noise or other silicate-related vibrations. For Fe-free glasses (i.e., no peak at 372 cm^{-1}), the S oxidation state can be quantified by using the height of the 990 and 2,574 cm^{-1} peaks after the spectra have been deconvolved. The peak heights are assumed to be proportional to the S concentration in the glass but not using the same proportionality factor, but this can be accounted for by creating a calibration curve [21].

5.2. Beam damage

Di Genova *et al.* [54] investigated beam damage during Raman spectroscopy (maximum beam conditions of 11 mW laser power and 26 min per analysis). Beam damage causes oxidation (increase in the intensity of the band associated with Fe^{3+} structural bonds at ~970 cm^{-1}), decrease in intensity of the H_2O (OH) peak, and nanolite formation (with a new peak at ~670 cm^{-1}). The change increased with increasing acquisition time or at higher laser powers and was more prominent in alkali- or Fe-rich samples. The intensity of the photon beam is far less than for XANES, hence laser heating is thought to cause the same reaction to occur as for XANES [54].

6. Synchrotron Mössbauer source (SMS) spectroscopy

6.1. Technique

Mössbauer spectroscopy uses the recoil-free resonant absorption of gamma rays to probe changes in the energy levels of an atomic nucleus in response to the surrounding electric and magnetic environment. Gamma rays over a narrow energy range are transmitted through the sample and the resulting absorption spectra give information on the coordination and oxidation state (Fig. 3d). Careful fitting of the spectra allows quantification of the Fe oxidation state and knowledge about the number of different environments of Fe within the glass structure [55]. This is a relatively simple mathematical procedure which is not directly dependent on comparison with standards [55]. In conventional Mössbauer spectroscopy for iron (^{57}Fe), a ^{57}Co radioactive source is moved over a range of velocities to produce gamma rays over the required energy range. These gamma rays are difficult to focus and relatively weak, therefore long measurement times (days) are needed and the resulting spatial resolution is poor. SMS spectroscopy uses synchrotron radiation, which gives a focussed (down to 10 μm), high brilliance gamma source allowing measurements in minutes [56].

6.2. Beam damage

There are currently no published studies investigating beam damage on glasses during SMS. SMS and XANES both use synchrotron-generated, highly-focussed photon beams for analysis. Hence, the mechanisms of beam damage and resultant changes to the glass would likely be similar (e.g., oxidation and reduction of Fe and H_2O loss). In contrast to XANES, SMS at a beamline such as ID18 at ESRF uses ^{57}Fe resonant gamma radiation generated by passing the synchrotron beam through an iron borate crystal. This mechanism also reduces the photon flux arriving at the sample by ~8 orders of magnitude, which negates the chance of beam damage that would result from XANES (pers. comm. Valerio Cerantola). For instance, the ID18 beamline at ESRF is reduced to a photon flux of 2×10^4 photons s^{-1} by the time it arrives at the sample. This is four orders of magnitude less than that the maximum flux observed to avoid beam damage on hydrous glass (~10^8 photons s^{-1}) at the I18 beamline at the Diamond Light Source [47, 56]. If higher photon fluxes are used for SMS, then similar problems to XANES might be expected.

7. Mitigation strategies

There are two approaches to mitigating beam damage: (1) change the analytical conditions such that beam damage is minimised or (2) modify data collection and processing techniques such that the analyses correct for any beam damage effects. In all cases, beam damage is more severe using higher beam densities (e.g., smaller beam size, higher beam current for electrons, higher intensity for photons). Hence, using lower beam densities reduces beam damage, but this sacrifices spatial resolution, increases analytical time, and/or decreases precision. In some cases this is acceptable, for instance using <5 mW laser power and <3 minutes analysis time for Raman spectroscopy can still produce good results with modern detectors [54]. For XANES, the photon flux must be heavily attenuated to eliminate beam damage in hydrous glasses, but reasonable errors on Fe oxidation state have been achieved by doing this [47]. For EPMA, mobile major elements are often analysed for short-times at the start of the analysis, when they have had little time to migrate, as their concentration is sufficiently high that precision is not compromised (e.g., [15]). Using a cold stage during EPMA can eliminate element migration [40], but has not been proven to prevent redox changes and has been shown to exacerbate these problems during XANES [48, 49].

If the glass sample size permits, the sample can be moved around constantly to analyse undamaged areas, an approach that has been used for Fe and S oxidation states [26, 34, 35]. Alternatively, TDI measurements can be extrapolated to time zero prior to beam damage, but this requires knowing what will change and how it will change. This approach has been applied to mobile element concentrations and Fe oxidation state determinations using EPMA and could perhaps be applied to XANES in the future [16, 42].

As beam damage results in changes to glass composition and structure, the order of analyses is critical to ensure reliable results. Ideally, the least damaging technique would be used but instrument access may not allow this. Raman can be used in such a way that beam damage does not occur, and hence can be used first even before polishing to reveal melt inclusions at the sample surface. H_2O easily migrates during EPMA and XANES, hence techniques such as FTIR and SIMS should be applied next as subsequent concentration and isotope measurements could be compromised. Although SMS and XANES are less damaging measurement techniques, the need for a thin, doubly polished wafer for analysis (not for all beamlines in the case of XANES) can make subsequent analyses challenging. Oxidation state measurements using EPMA should be carried out last (after standard EPMA), due to the high beam density required for analysis.

8. Conclusions

EPMA, XANES, Raman, and EELS can all cause reduction or oxidation of Fe and S in silicate glass. The rate and direction of redox change depends on the primary beam conditions (e.g., beam type, accelerating voltage, beam current, photon flux, laser power, etc.) and measurement time, but also on glass composition (e.g., Si, Fe, and H_2O). For EPMA alkali-poor anhydrous glass reduces, whilst alkali-rich or hydrous glass oxidises. Conversely, for XANES Fe-poor glass reduces, whilst Fe-rich glass oxidises. Broadly, increased H_2O, alkalis, or Fe increases the rate of redox change with both electron and photon beams. Oxidation is caused by cation migration in response to: electric field formation due to electron addition (EPMA) or removal (EELS), photon-induced bond breaking (XANES), or sample heating (Raman). The beam conditions for SMS appear to be too low to cause beam damage. More data are required to understand Fe redox changes in EELS, Raman, and SMS; and S redox changes in EPMA and XANES. The simplest way to mitigate beam damage is to reduce beam density during analysis, although moving the sample and time-dependent intensity methods can also be used. Careful consideration of analytical sequence and conditions can allow the glass to be analysed multiple times using a variety of techniques to fully characterise silicate glass samples.

Acknowledgements

We would like to thank Valerio Cerantola and Alexandr Chumakov for their comments on the SMS section, Jon Wade for his helpful review that greatly improved the manuscript, and Bjørn Sørensen for his editorial handling.

References

[1] Kress V C and Carmichael I S E 1991 The compressibility of silicate liquids containing Fe_2O_3 and the effect of composition, temperature, oxygen fugacity and pressure on their redox states. *Contrib. Mineral. Petrol.* **108** 82-92
[2] Jugo P J, Wilke M and Botcharnikov R E 2010 Sulfur K-edge XANES analysis of natural and synthetic basaltic glasses: Implications for S speciation and S content as function of oxygen fugacity . *Geochim. Cosmochim. Acta* **74** 5926-5938
[3] Wilke M 2005 Fe in magma - An overview. *Ann. Geophys.* **48** 609-617
[4] Vicenzi E P, Green T and Sie S 1994 Effect of oxygen fugacity on trace-element partitioning between immiscible silicate melts at atmospheric pressure: A proton and electron microprobe study. *Chem. Geol.* **117** 355-360
[5] Tattitch B and Blundy J D 2017 Partitioning of Cu and Mo between felsic melts and saline magmatic fluids: influence of salinity, fO_2 and fS_2. *Appl. Earth Sci.* **126**. 99
[6] Cukierman M and Uhlmann D R 1974 Effects of iron oxidation state on viscosity, lunar composition 15555. *J. Geophys. Res.* **79** 1594-1598
[7] Dingwell D B and Virgo D 1987 The effect of oxidation state on the viscosity of melts in the system Na_2O-FeO-Fe_2O_3-SiO_2. *Geochim. Cosmochim. Acta* **51** 195-205
[8] Hamilton D L, Burnham C W and Osborn E F 1964 The solubility of water and effects of oxygen fugacity and water content on crystallization in mafic magmas. *J. Petrol.* **5** 21-39

[9] Carmichael I S E and Ghiorso M S 1990 The effect of oxygen fugacity on the redox state of natural liquids and their crystallizing phases. *Rev. Mineral. Geochem.* **24** 191-212
[10] Bouhifd M A, Richet P, Besson P, Roskosz M and Ingrin J 2004 Redox state, microstructure and viscosity of a partially crystallized basalt melt. *Earth Planet. Sci. Lett.* **218** 31-44
[11] Kolzenburg S, Di Genova D, Giordano D, Hess K U and Dingwell D B 2018 The effect of oxygen fugacity on the rheological evolution of crystallizing basaltic melts. *Earth Planet. Sci. Lett.* **487** 21-32
[12] Humphreys M C S, Brooker R A, Fraser D G, Burgisser A, Mangan M T and McCammon C 2015 Coupled interactions between volatile activity and Fe oxidation state during arc crustal processes. *J. Petrol.* **56** 795-814
[13] Kelley K A and Cottrell E 2009 Water and the oxidation state of subduction zone magmas. *Science* **325** 605-607
[14] Roedder E 1979 Origin and significance of magmatic inclusions. *Bull. Mineral.* **102** 487-510
[15] Blundy J D and Cashman K V 2008 Petrologic reconstruction of magmatic system variables and processes. *Rev. Mineral. Geochem.* **69** 179-239
[16] Hughes E C, *et al.* 2018 High spatial resolution analysis of the Iron oxidation state in silicate glasses using the electron probe. *Amer. Mineralogist* **103** 1473-1486
[17] Wilke M, Klimm K and Kohn S C 2011 Spectroscopic studies on sulfur speciation in synthetic and natural glasses. *Rev. Mineral. Geochem.* **73** 41-78
[18] Cottrell E, Kelley K A, Lanzirotti A and Fischer R A 2009 High-precision determination of iron oxidation state in silicate glasses using XANES. *Chem. Geol.* **268** 167-179
[19] Burgess K D, Stroud R M, Dyar M D and McCanta M C 2016 Submicrometer-scale spatial heterogeneity in silicate glasses using aberration-corrected scanning transmission electron microscopy. *Amer. Mineraogist* **101** 2677-2688
[20] Di Genova D, Hess K U, Chevrel M O and Dingwell D B 2016 Models for the estimation of Fe^{3+}/Fe_{tot} ratio in terrestrial and extraterrestrial alkali- and iron-rich silicate glasses using Raman spectroscopy. *Amer. Mineralogist* **101** 943-952
[21] Klimm K, Kohn S C, O'Dell L A, Botcharnikov R E and Smith M E 2012 The dissolution mechanism of sulphur in hydrous silicate melts. I: Assessment of analytical techniques in determining the sulphur speciation in iron-free to iron-poor glasses. *Chem. Geol.* **322-323** 237-249
[22] de Groot F 2001 High-resolution X-ray emission and X-ray absorption spectroscopy. *Chem. Rev.* **101** 1779-1808
[23] Hofer H E and Brey G P 2007 The iron oxidation state of garnet by electron microprobe: Its determination with the flank method combined with major-element analysis. *Amer. Mineralogist* **92** 873-885
[24] Smith D G W and O'Nions R K 1971 Investigations of the $L_{II,III}$ X-ray emission spectra of Fe by the electron microprobe Part I: Some aspects of the Fe $L_{II,III}$ spectra from metallic iron and haematite. *J. Phys. D: Appl. Phys.* **4** 320
[25] Gopon P, Fournelle J, Sobol P E and Llovet X 2013 Low-voltage electron-probe microanalysis of Fe-Si compounds using soft X-rays. *Microsc. Microanal.* **19** 1698-1708
[26] Zhang C, *et al.* 2018 Electron microprobe technique for the determination of iron oxidation state in silicate glasses. *Amer. Mineralogist* **103** 1445-1454
[27] Hofer H E, Brey G P, Schulz-Dobrick B and Oberhansli R 1994 The determination of the oxidation state of iron by the electron microprobe. *Eur. J. Mineral.* **6** 407-418
[28] Fialin M, Bézos A, Wagner C and Humler E 2004 Quantitative electron microprobe analysis of $Fe^{3+}/\Sigma Fe$: Basic concepts and experimental protocol for glasses. *Amer. Mineralogist* **89** 654-662
[29] Hofer H E 2002 Quantification of Fe^{2+}/Fe^{3+} by electron microprobe analysis - New developments. *Mössbauer Spectrosc.* **144-145** 239-248

[30] Di Genova D, Caracciolo A and Kolzenburg S 2018 Measuring the degree of 'nanotilization' of volcanic glasses: Understanding syn-eruptive processes recorded in melt inclusions. *Lithos* **318-319** 209-218
[31] Carroll M R and Rutherford M J 1998 Sulfur speciation in hydrous experimental glasses of varying oxidation state: Results from measured wavelength shifts of sulfur X-rays. *Amer. Mineralogist* **73** 845-849
[32] Wallace P J and Carmichael I S E 1992 Sulfur in basaltic magmas. *Geochim. Cosmochim. Acta* **56** 1863-1874
[33] Wilke M, *et al.* 2008 The origin of S^{4+} detected in silicate glasses by XANES. *Amer. Mineralogist* **93** 235-240
[34] Rowe M C, Kent A J R and Nielsen R L 2007 Determination of sulfur speciation and oxidation state of olivine hosted melt inclusions. *Chem. Geol.* **236** 303-322
[35] Métrich N and Clocchiatti R 1996 Sulfur abundance and its speciation in oxidized alkaline melts. *Geochim. Cosmochim. Acta* **60** 4151-4160
[36] Bonnelle C 2004 Charge trapping in dielectrics. *Microsc. Microanal.* **10** 691-696
[37] Cazaux J 1996 Electron probe microanalysis of insulating materials: Quantification problems and some possible solutions. *X-ray Spectrom.* **25** 265-280
[38] Humphreys M C S, Kearns S L and Blundy J D 2006 SIMS investigation of electron-beam damage to hydrous, rhyolitic glasses: Implications for melt inclusion analysis. *Amer. Mineralogist* **91** 667-679
[39] Morgan G B and London D 2005 Effect of current density on the electron microprobe analysis of alkali aluminosilicate glasses. *Amer. Mineralogist* **90** 1131-1138
[40] Kearns S L, Steen N and Erlund E 2002 Electron probe microanalysis of volcanic glass at cryogenic temperatures. *Microsc. Microanal.* **8** (Suppl. 2) 1562-1563
[41] Henderson G S, Calas G and Stebbins J F 2006 The structure of silicate glasses and melts. *Elements* **2** 269-273
[42] Nielsen C H and Sigurdsson H 1981 Quantitative methods for electron microprobe analysis of sodium in natural and synthetic glasses. *Amer. Mineralogist* **66** 547-552
[43] Fialin M and Wagner C 2012 Redox kinetics of iron in alkali silicate glasses exposed to ionizing beams: Examples with the electron microprobe. *J. Non. Cryst. Solids* **358** 1617-1623
[44] Nishida T 1995 Mössbauer effect in inorganic glasses. *Hyperfine Interact.* **95** 23-39
[45] Jugo P J , Luth R W and Richards J P 2005 Experimental data on the speciation of sulfur as a function of oxygen fugacity in basaltic melts. *Geochim. Cosmochim. Acta* **69** 497-503
[46] Shorttle O, Moussallam Y, Hartley M E, Maclennan J, Edmonds M and Murton B J 2015 Fe-XANES analyses of Reykjanes Ridge basalts: Implications for oceanic crust's role in the solid Earth oxygen cycle. *Earth Planet. Sci. Lett.* **427** 272-285
[47] Moussallam Y, *et al.* 2019 Mantle plumes are oxidised. *Earth Planet. Sci. Lett.* **527** 115798
[48] Gonçalves Ferreira P, de Ligny D, Lazzari O, Jean A, Cintora Gonzalez O and Neuville D R 2013 Photoreduction of iron by a synchrotron X-ray beam in low iron content soda-lime silicate glasses. *Chem. Geol.* **346** 106-112
[49] Cottrell E, *et al.* 2018 A Mössbauer-based XANES calibration for hydrous basalt glasses reveals radiation-induced oxidation of Fe. *Amer. Mineralogist* **103** 489-501
[50] Moussallam Y, *et al.* 2014 Tracking the changing oxidation state of Erebus magmas, from mantle to surface, driven by magma ascent and degassing. *Earth Planet. Sci. Lett.* **393** 200-209
[51] Fiege A, *et al.* 2017 Calibration of Fe XANES for high-precision determination of Fe oxidation state in glasses: Comparison of new and existing results obtained at different synchrotron radiation sources. *Amer. Mineralogist* **102** 369-380
[52] Thomas R 2000 Determination of water contents of granite melt inclusions by confocal laser Raman microprobe spectroscopy. *Amer. Mineralogist* **85** 868-872

[53] Di Muro A, Métrich N, Mercier M, Giordano D, Massare D and Montagnac G 2009 Micro-Raman determination of iron redox state in dry natural glasses: Application to peralkaline rhyolites and basalts. *Chem. Geol.* **259** 78-88
[54] Di Genova D, Sicola S, Romano C, Vona A, Fanara S and Spina L 2017 Effect of iron and nanolites on Raman spectra of volcanic glasses: A reassessment of existing strategies to estimate the water content. *Chem. Geol.* **475** 76-86
[55] Mysen B O, Carmichael I S E and Virgo D 1985 A comparison of iron redox ratios in silicate glasses determined by wet-chemical and ^{57}Fe Mössbauer resonant absorption methods. *Contrib. Mineral. Petrol.* **90** 101-106
[56] Potapkin V, *et al.* 2012 The ^{57}Fe synchrotron Mössbauer source at the ESRF. *J. Synchrotron Radiat.* **19** 559-569